ICMIEE-PI-140105

Characteristics of flow over three side-by-side square prisms

Qinmin Zheng[1], *Md. Mahbub Alam*[1,2,*], *Yu Zhou*[1]
[1]Institute for Turbulence-Noise-Vibration Interaction and Control, Shenzhen Graduate School
Harbin Institute of Technology, Shenzhen, China
[2]Key Kab of Advanced Manufacturing and Technology, Shenzhen Graduate School
Harbin Institute of Technology, Shenzhen, China

ABSTRACT
A low-Reynolds number (Re = 150) flow over three side-by-side square prisms placed normal to the oncoming flow is simulated systematically at L/W = 1.2 ~ 8.0, using finite volume method, where L is the prism center-to-center spacing and W is the prism width. Six distinct flow structures and their ranges are identified, viz., single-bluff-body flow (L/W < 1.5), flip-flopping flow (1.5 ≤ L/W < 2.0), symmetrically-biased coupled flow (2.0 ≤ L/W ≤ 2.5), transition flow (2.5 < L/W < 3.0), non-biased coupled flow (3.0 ≤ L/W ≤ 7.0) and non-biased weakly coupled flow (L/W > 7.0). Physical aspects of each flow regime, such as vortex structures, gap flow deflections, shedding frequencies are discussed in detail. A secondary frequency other than the Strouhal number (primary frequency) is identified in symmetrically biased and non-biased coupled flow regimes. The origin and effect of the secondary frequency on lift forces are unearthed. These results, most of which have been obtained for the first time, are of fundamental significance.

Keywords: flow-structure interactions, three side-by-side square prisms, vortex streets, secondary frequency

1. Introduction

The square prism is the representative model of bluff bodies with sharp corners, characterized by a fixed flow separation point. However, in spite of its great importance to engineering, the flow around multiple square prisms has received much less attention than that of circular cylinders.

Alam *et al.*[1] at $Re = 4.7\times10^4$ performed systematic measurements of the flow field, Strouhal number St, and time-averaged and fluctuating forces for two side-by-side square prisms at L/W = 1.02 ~ 6.00. Four distinct flow regimes, namely (i) single-body regime (1.0 < L/W < 1.3), (ii) two-frequency regime (1.3 ≤ L/W ≤ 2.2), (iii) transition regime (2.2 < L/W < 3.0), and (iv) coupled vortex street regime (L/W ≥ 3.0) are identified. Besides, the interference between shear layers, the gap flow deflection and changeover, flow entrainment, recirculation bubble, vortex interactions and formation lengths for each regime, are studied in detail and connected to the characteristics of the time-averaged and fluctuating fluid forces. At much smaller Re = 300, Alam & Zhou [2] observed qualitatively similar results in flow visualization experiments.

Kumar *et al.* [3] simulated the flow around a row of nine square prisms at Re = 80 for L/W = 1.3 ~ 13.0, using lattice-Boltzmann method. Three flow regimes are recognized based on vorticity fields and drag coefficient signals: synchronized flow, quasi-periodic flow and chaotic flow. No significant interaction between the wakes is observed at L/W > 7.

In the present work, we focus on detailed physics of the flow over three side-by-side square prisms. Simulations are performed at Re = 150 for L/W = 1.2 ~ 8.0 covering all possible flow regimes. Vorticity fields, shedding frequencies along with the time series of lift force are analyzed to explicitly delineate the resultant flow structures.

2. Numerical methods

2.1. Computational models and boundary conditions

The dimensionless 2-D N-S equations governing the flow of a Newtonian fluid can be written in vector form as

$$\left.\begin{aligned}\frac{\partial\vec{U}}{\partial t}+\left(\vec{U}\cdot\nabla\right)\vec{U}&=-\nabla P+\frac{1}{Re}\nabla^2\vec{U}\\ \nabla\cdot\vec{U}&=0\end{aligned}\right\} \qquad (1)$$

where Re is the Reynolds number based on free-stream velocity U_∞ and prism width W. Re is kept constant at 150. In solving the governing equations, the different physical quantities are normalized by U_∞ and/or W. The finite volume method is applied on structured meshes. The pressure-velocity coupling is handled with the semi-implicit pressure linked equations (SIMPLE) scheme. Discretization of the convective terms in the conservation equations is accomplished through a second-order accurate upwind differencing scheme. Second-order implicit forward discretization is adopted for the time derivative term in order to accelerate the convergence process.

Fig. 1 shows a schematic diagram of the computational domain and grid distribution around a quadrant of a prism. As presented in Fig. 1(a), the computational domain is chosen to be $(30W + 3L) \times (40W + L)$ with

*Corresponding author.
Email address: alamm28@yahoo.com; alam@hitsz.edu.cn

the upstream and downstream boundaries located at $12W + 0.5L$ and $28W + 0.5L$, respectively, from the coordinate origin at the center of the middle prism. The lateral surfaces are located at $15W + 1.5L$ each from the origin. At the inlet, a uniform velocity profile ($u = 1, v = 0$) is imposed, while the stress vector is set to zero at the outlet boundary. On the upper and lower boundaries, the component of the velocity normal to, and the component of the stress vector along the boundaries are prescribed a zero value. No-slip boundary condition ($u = v = 0$) is employed on the surfaces of the square prisms. In the computation domain, the initial flow velocities (at $t = 0$) are given as $u = U_\infty$, $v = 0$.

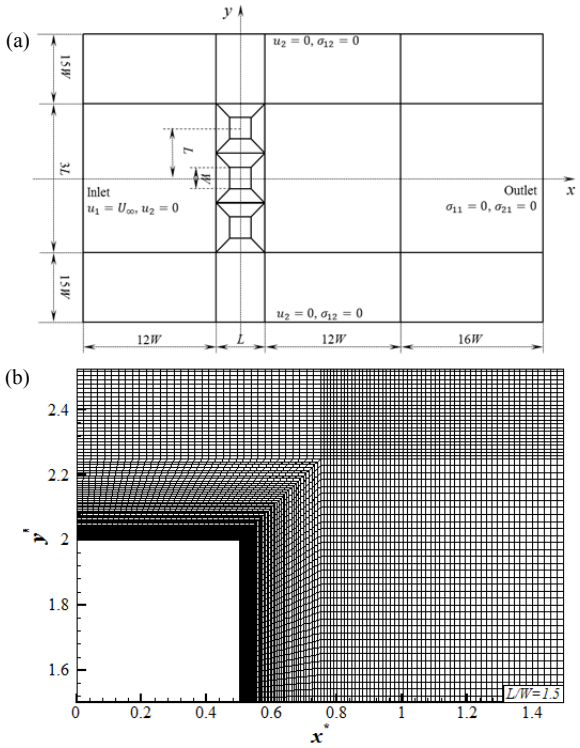

Fig. 1 (a) Sketch of the computational domain and boundary conditions, and (b) grid distribution around a quadrant of a prism.

2.2. Grid independence test and result validation

Grid independence test for the flow around a single square prism was carried out before the extensive simulations, where the computational domain and grid distribution of the prism are made similar to those of three side-by-side square prisms. Table 1 compares C_L', $\overline{C_D}$, C_D', and St obtained from the present and previous simulations for a single square prism at $Re = 150$.

Table 1 Grid independence test for single prism at $Re = 150$

Case	C_L'	$\overline{C_D}$	C_D'	St
Present	0.2721	1.4799	0.0167	0.1576
Saha *et al.*[4]	0.2740	-	0.0170	-
Sohankar *et al.* [5]	0.2300	1.4400	-	0.1650
Kumar *et al.* [3]	-	1.5200	-	0.1570
Sharma *et al.* [6]	-	1.4700	-	0.1560

Overall, C_L', $\overline{C_D}$, C_D', and St results display a good accordance with those in the literatures.

3. Flow structure

$L/W = 1.2$ was simulated first and increased successively to 8.0. The prisms at $L/W = 8.0$ behaved almost independently and a weak interaction was observed between the adjacent wakes. So less attention will be paid to the results at this L/W. The wakes interact each other in a complicated manner at $L/W \leq 7.0$, resulting in six distinct flow structures: (A) single-bluff-body flow ($L/W < 1.5$), (B) flip-flopping flow ($1.5 \leq L/W < 2.0$), (C) symmetrically-biased coupled flow ($2.0 \leq L/W \leq 2.5$), (D) transition flow ($2.5 < L/W < 3.0$), (E) non-biased coupled flow ($3.0 \leq L/W \leq 7.0$) and (F) non-biased weakly coupled flow ($L/W > 7.0$). Each regime has distinct intrinsic features associated vortex structures, shear layer behaviors, gap flow deflections, shedding frequencies and force characteristics.

Fig. 2 shows the contours of non-dimensional instantaneous vorticity patterns at different regimes. The single-bluff-body flow (regime A) prevails at $L/W < 1.5$, where vortex shedding occurs essentially from the outer shear layers of the outer prisms (Fig. 2a); a single vortex street, thus, forms behind the three prisms, similarly to that of a single bluff body. Although weak, flows through the two gaps are apparent and are prone to bias toward the growing vortex. When the vortex from the lower side grows, both gap flows swerve to the lower side. In the next half cycle of the vortex shedding, the upper vortex will grow and pull the gap flows toward the upper side.

When L/W is increased to regime B ($1.5 \leq L/W < 2.0$), a greater amount of flow can pass through the gaps and can split the wake into three immediately downstream of the prisms. Appreciable vortices from the gap sides form around the prisms. The vortices merge with the outer vortices shed from the outer prisms. The gap flow now can flip-flop randomly at different fashions to be biased upward (Fig. $2b_1$), downward (Fig. $2b_2$), inward (Fig. $2b_3$) and outward (Fig. $2b_4$), generating four different flow structures.

The symmetrically-biased coupled flow occurring at $2.0 \leq L/W \leq 2.5$ (regime C) is characterized by the gap flow biased/diverged outward symmetrically (Fig. 2c). A substantial wide wake thus accompanies the middle prism and a narrow wake complements each outer prism. This flow structure is very similar to that in Fig. $2(b_4)$, implying that the flow structure change from regimes B to C is continuous. The vortices shedding from the outer prisms are found to be perfectly coupled with a constant phase lag $\phi = 180°$ (antiphase). Note that here coupling means the coupling between the vortices from the outer prisms only, as the middle prism shedding frequency is always different from the outer prisms. It was found that the mean base-pressure of the outer prisms was identical and much smaller than that of the middle prism. Since

the gap width is now large enough, the narrow wake associated with low base pressure can pull only the nearest shear layer of the middle prism. The gap flows are thus stably biased outward, not prone to switch.

In the non-biased coupled flow regime ($3.0 \le L/W \le 7.0$, regime E), the gap flows are no longer biased. Unlike other flow regimes A-D, a single vortex street, qualitatively similar to that behind an isolated prism, persists behind each prism. Again the vortex sheddings from the outer prisms occurring at the same frequency are coupled with a fixed ϕ. The vortex shedding frequency of the middle prism is however different, slightly higher than that of the outer prisms. The instantaneous phase relationship between the vortex sheddings from the middle and outer prisms thus changes periodically from anti-phase (Fig. $2d_1$) to in-phase (Fig. $2d_2$), and vice versa, which has a great impact on the time histories of lift forces of the prisms. It is noted that the phase lag between the vortex sheddings from outer prisms depends on L/W; ϕ decaying from 110° to 0° between $L/W = 3.0$ and 3.5 remains 0° at $3.5 \le L/W \le 4.0$ before increasing gradually to 80° at $L/W = 7.0$. In the latter L/W range, the interaction between the wakes weakens, leading to the change in the phase lag.

Regime D ($2.5 < L/W < 3.0$) is the transition between regimes C and E, where the modification of the flow from symmetrically-biased to non-biased is discontinuous; both flow modes perhaps appear intermittently in this regime. Alam *et al.*[1] for two side-by-side square prisms observed similar transition regime where biased and coupled flows switched from one to the other.

At $L/W > 7.0$, the coupling between the outer wakes is weak and each prism tends to behave like a single prism with difference in frequencies between the middle and outer prisms getting smaller. This regime, hence, can be regarded as weak-interaction or non-biased weakly coupled flow regime.

4. Shedding frequency

The power spectra of fluctuating lifts of the three prisms at different regimes are shown in Fig. 3. Here prisms 1, 2 and 3 refer to the upper, middle and lower prisms, respectively. For single-bluff-body flow, identical $St = 0.068$ is observed for the three prisms (Fig. 3a), implying that vortices are separated at the same frequency from the freestream sides of the prisms and generate a single Karman vortex street behind the three prisms. $St = 0.0821$ may be associated with the influence of the gap flow. The remaining peaks are the harmonic and linear combinations of these two frequencies.

In the flip-flopping flow, though the gap flows are biased and flip-flop, a single combined wake dominantly forms behind the three prisms. The flows through the gaps acting as base bleeds postpone the vortex formation from the free stream sides, *St* thus jumps to 0.1504 (Fig. 3b). The peaks corresponding to the *St* are relatively wider than those in the other regimes, because of the random switch of the gap flows.

The narrow wakes behind the outer prisms in the symmetrically-biased coupled flow are connected to a *St* of 0.1896 (Fig. 3c), while the wide wake behind the middle prism is associated with a smaller and higher $St = 0.1505$ and 0.2288. The $St = 0.1505$ is due to a tendency of shedding corresponding to the wide wake, while $St = 0.2288$ results from a strong alternate coupling of vortices in the two gaps. Different from the single-bluff-body and flip-flopping flows, a very low frequency ($St = 0.0390$) with a tiny peak (see the insets) is found in this regime. It is referred to as a secondary frequency hereafter. Indeed, $St = 0.0390$ is the difference between $St = 0.1896$ and 0.1505. The secondary frequency has a great influence to make a beat-like variation in the time histories of lift forces of the prisms. The origin of the secondary frequency and its effect will be discussed more detailed later. The secondary frequency will be more obvious in the non-biased coupled flow.

When the gap flows are not biased (non-biased coupled flow), the low *St* of the middle prism jumps and the high *St* disappears. The difference in *St* between the middle and outer prisms becomes smaller (Fig. 3d). Here the middle prism *St* is larger than that of the outer prisms, resulted from the higher mean velocity in the shear layers of the middle prism. The peak at $St = 0.0116$ is again associated with the secondary frequency.

5. Physics of the secondary frequency

As mentioned above, the shedding frequencies of the outer prisms are identical, but higher at symmetrically -biased coupled flow and smaller at non-biased coupled flow than that of the middle prism. It would be interesting to see how the flow classification is connected to *St*. Variations in *St* of the three prisms are shown in Fig. 4(a). While *St*(s) of the all three prisms are identical and very small in regime A, they remaining identical jumps to a higher value in regime B. The middle and outer prisms have however different *St* in regime C, smaller for the middle prism. *St* again jumps in the transition regime D, before tapering off slowly with L/W in the regime E where *St* is larger for the middle prism than outer prisms. The difference in *St* between the middle and outer prisms is small in regime F. The difference in the frequencies between the middle and outer prisms in regimes C, D, E and F may be connected to difference in velocities between the gaps and outer sides. Therefore, the average of time-mean streamwise velocities at the two sides (see the inset) of each prism, U_{avg}, is estimated and plotted concurrently in Fig. 4(a). What is interesting here is that U_{avg} follows the *St* behavior, being smaller for the middle prism in regime C

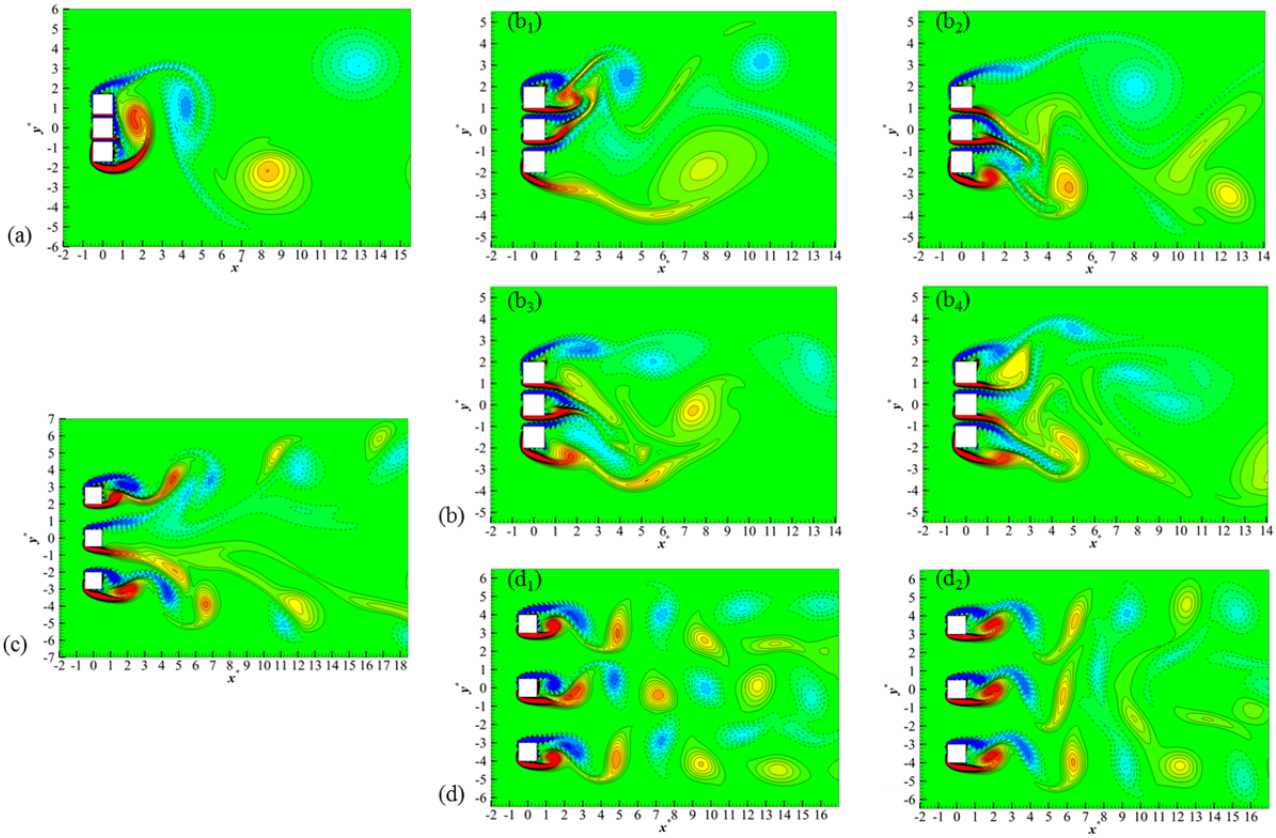

Fig. 2 Contours of vorticity at (a) $L/W = 1.2$ (single bluff body flow, regime A, $L/W < 1.5$); (b) $L/W = 1.5$ (flip-flopping flow, regime B, $1.5 \le L/W < 2.0$): the gap flows biased (b_1) upward, (b_2) downward, (b_3) inward, (b_4) outward; (c) $L/W = 2.5$ (symmetrically-biased coupled flow, regime C, $2.0 \le L/W \le 2.5$); (d) $L/W = 3.5$ (non-biased coupled flow, regime E, $3.0 \le L/W \le 7.0$): the middle prism shedding (d_1) anti-phase and (d_2) in-phase with the others. Transition flow (regime D, $2.5 < L/W < 3.0$) and non-biased weakly coupled flow (regime F, $L/W > 7$) are not shown here.

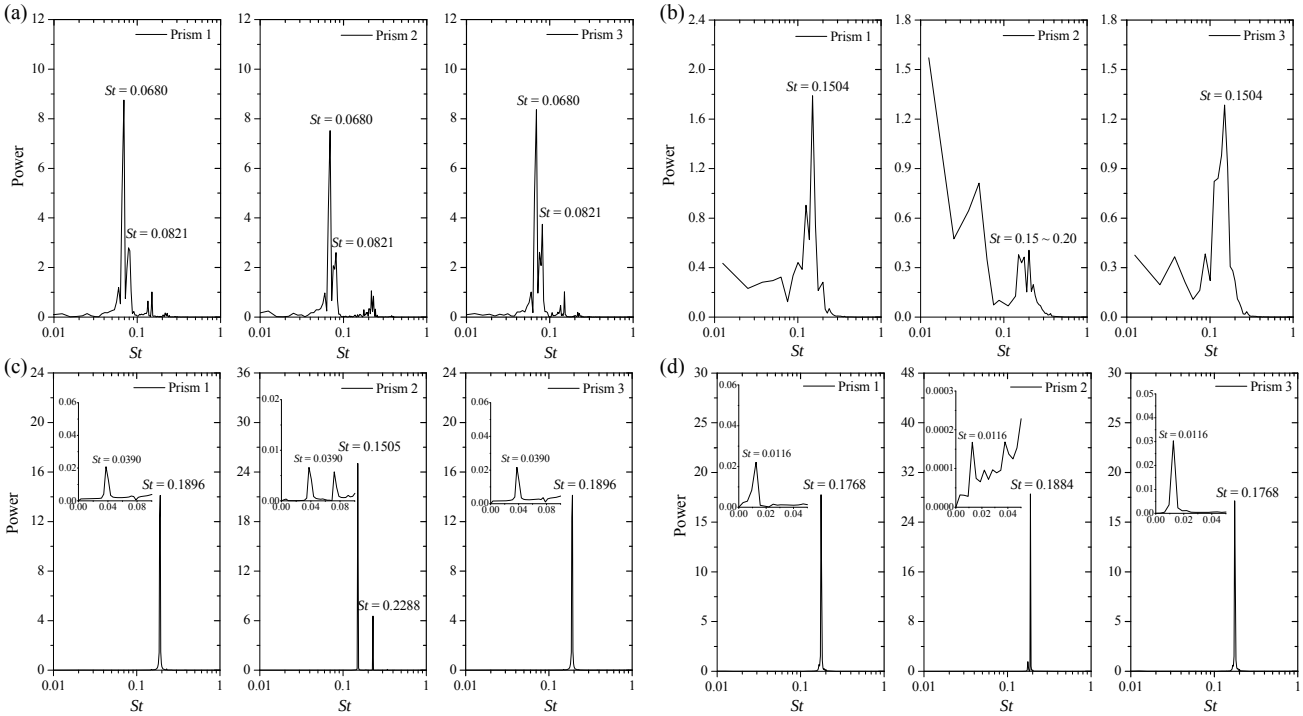

Fig. 3 Power spectra of fluctuating lift at (a) $L/W = 1.2$ (regime A, $L/W < 1.5$), (b) $L/W = 1.5$, (regime B, $1.5 \le L/W < 2.0$), (c) $L/W = 2.5$ (regime C, $2.0 \le L/W \le 2.5$), (d) $L/W = 3.5$, (regime E, $3.0 \le L/W \le 7.0$). Power is in arbitrary units.

where *St* is smaller, and greater in regime E where *St* is larger, all compared to those of the counterpart outer prisms.

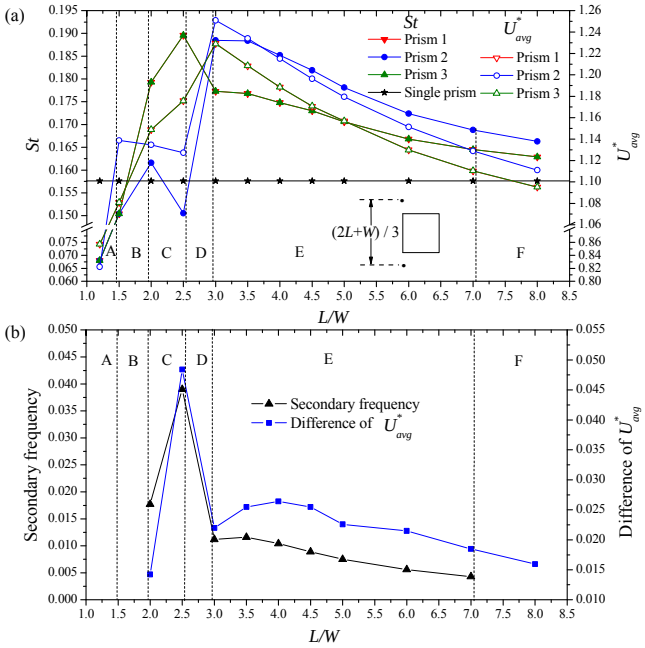

Fig. 4 (a)Variation of shedding frequency (*St*) and U^*_{avg} with *L/W*. (b) Variation of the secondary frequency and difference of U^*_{avg} between the outer and middle prisms with *L/W*. $U^*_{avg} = U_{avg}/U_\infty$.

Table 2 Variation in Strouhal number (middle prism) based on U_∞ and U_{gap} as a function of *L/W*.

L/W	fW/U_∞	U_{gap}/U_∞	fW/U_{gap}
2.0	0.1616	1.1346	0.1424
2.5	0.1505	1.1273	0.1335
3.0	0.1885	1.2509	0.1507
3.5	0.1884	1.2340	0.1527
4.0	0.1852	1.2151	0.1524
4.5	0.1819	1.1963	0.1521
5.0	0.1781	1.1795	0.1510
6.0	0.1724	1.1513	0.1497
7.0	0.1688	1.1289	0.1495
8.0	0.1663	1.1111	0.1497

To check the argument about the effect of U_{avg} on *St*, modified *St* based on U_{gap} (= U_{avg}) is calculated for the middle prism as presented in Table 2. While *St* based on U_∞ varies from 0.1505 to 0.1885, the modified *St* based on U_{gap} collapses to about ≈ 0.15, with a small departure at *L/W* = 2.0 and 2.5. The departure may be due to fact that since the gap flow is highly biased outward, the U_{gap} measurement location lies in the shear layer. In overall, it can be concluded that *St* of the middle prism is primarily influenced by the flow velocity around the prism and is proportional to U_{gap}.

Figure 4(b) displays the secondary frequency and difference in U_{avg} between the middle and outer prisms. They both follow the same trend, confirming that the secondary frequency is somehow associated with the difference in *St* or U_{avg} in turn between the middle and outer prisms.

6. The origin of the secondary frequency and its effect on C_L

From the power spectrum results, it has been observed that C_L signals at the symmetrically-biased and non-biased flow regimes have a short (Strouhal or primary frequency,) and long (secondary frequency) periods. The amplitude associated with the long period is small compared to that with the short period. Fig. 5 shows time histories of lifts of the three prisms at *L/W* = 3.5. The short period is easily understood, while a beat-like change in C_L amplitude is also obvious, with maximum, minimum and again maximum amplitudes around time *t* = 114.2, 118.0 and 122.9 seconds, respectively. This beat period is therefore about 8.7 seconds, corresponding to *St* = 0.0118, very close to the secondary *St* = 0.0116 obtained in the power spectrum (Fig. 3d). It thus proves that the beat phenomenon is associated with the secondary frequency. As we know from sound/light interference, a beat occurs when two sound/light waves of two different frequencies interact each other and the beat frequency is equal to the difference of the two frequencies. Here we observed the same phenomenon; the secondary/beat frequency is the difference in the shedding frequencies of the middle and outer prisms. It may be interesting to view representative flow structures at maximum and minimum amplitudes (associated with the secondary frequency) of C_L. Indeed the flow structures presented in Figs. 2(d_1) and (d_2) correspond to the maximum and minimum amplitude of C_L (*t* = 114.2 and 118.0 seconds, respectively) associated with the secondary frequency and at the same time both flow structures correspond to a maximum C_L associated with the primary frequency of the middle prism, as indicated by vertical lines. Interestingly, maximum C_L associated with the secondary frequency occurs when an in-phase shedding occurs from the two sides of a gap (Fig. 2d_1). On the other hand, an anti-phase shedding from the two sides of a gap results in a minimum C_L associated with the secondary frequency (Fig. 2d_2). Fortuitously, both gaps have the in-phase shedding (Fig. 2d_1) and antiphase shedding (Fig. 2d_2) at this *L/W*, as the shedding phase lag between the outer prisms was a constant of ≈ 0°. C_L(s) of the three prisms, associated with the secondary frequency, are thus reaching maximum or minimum simultaneously. When the phase lag between the outer prisms is ≠ 0°, maximum or minimum C_L of the three prisms does not occur simultaneously. So the beat/secondary frequency results from a continuous change in the phase lag between the sheddings from the two sides of a gap, from in-phase to

anti-phase, anti-phase to in-phase, and so on. Due to the different shedding frequencies from the two sides of a gap, the phase lag changes in every primary period. It should not be confused that when the shedding frequencies are different, how can the phase lag be obtained? Here the phase lag means the phase of the longer period shedding with respect to that of the shorter period shedding, i.e., considering the shorter period as a reference complete cycle period.

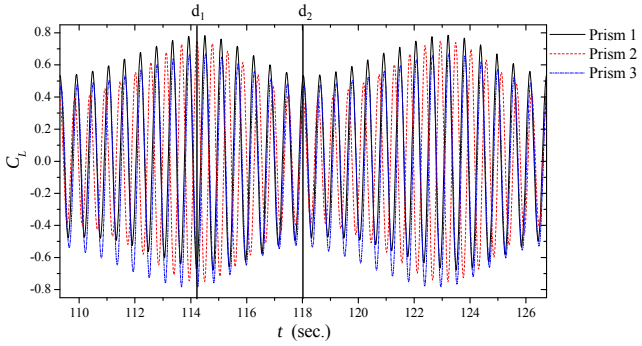

Fig. 5 The time histories of lift signals of the three prisms at $L/W = 3.5$. Note that the vertical lines d_1 and d_2 correspond to the wake structure presented in Fig. 1(d_1) and (d_2), respectively.

7. Conclusions

Based on vortex structure, fluid force and shedding frequencies, six distinct flow regimes have been identified. (i) Single-bluff-body flow (regime A) identified at $L/W < 1.5$ is characterized by vortex shedding from the freestream sides only, forming a single Karman vortex street with an identical *St*. (ii) Flip-flopping flow (regime B) appears at $1.5 \leq L/W < 2.0$ where the gap flows gain adequate strength to split the wake into three immediately downstream, but the three wakes merge into one shortly. Again a single *St* persists in the wake. The two gap flows flip-flop, both to be biased upward, downward, inward, and outward. (iii) Symmetrically-biased coupled flow (regime C, $2.0 \leq L/W \leq 2.5$) features with the two gap flows deflecting outward symmetrically, forming one wide wake of smaller *St* behind the middle prism and two narrow wakes of a larger *St* behind the two outer prisms. (iv) Transition flow ($2.5 < L/W < 3.0$, regime D) occurring between regimes C and E displays a remarkable jump in *St* of the middle prism and drop in *St* of outer prisms associated with a discontinuous change in the flow between regimes C and E. (v) The non-biased coupled flow (regime E) taking place at $3.0 \leq L/W \leq 7.0$ is exemplified by the fact that the gap flows are not biased anymore; the wake behind each prism is similar to that of an isolated prism. The sheddings from the outer prisms are coupled with a constant phase lag and identical *St*. The *St* of the middle prism is however different, higher than that of the outer prisms, both *St* decreasing with an increase in *L/W*. (vi) Non-biased weakly coupled flow (regime F, $L/W > 7.0$), where the difference in *St* between the middle and outer prisms is smaller and the interaction between the adjacent wake is weak.

A secondary frequency is observed in the symmetrically -biased and non-biased coupled flows, equal to the difference in shedding frequencies of the middle and outer prisms. The flow in the gap receives an interaction of the two frequencies, resulting in the secondary frequency. The secondary frequency has a great impact on the time series of the lift force to have a beat-like change, where the lift force associated with the beat is maximum when the sheddings from the two sides of a gap are inphase, and reaches a minimum when they are antiphase.

Acknowledgments

Alam wishes to acknowledge supports given to him from the Research Grant Council of Shenzhen Government through grants JCYJ20120613145300404 and JCYJ20130402100505796.

REFERENCES

[1] M. M. Alam, Y. Zhou, X. W. Wang, The wake of two side-by-side square cylinders, *Journal of Fluid Mechanics*, Vol. 669, pp 432-471, (2011).

[2] M. M. Alam and Y. Zhou, Intrinsic features of flow around two side-by-side square cylinders, *Physics of Fluids*, Vol. 25, pp 085106-1-21, (2013).

[3] S. R. Kumar, A. Sharma and A. Agrawal, Simulation of flow around a row of square cylinders, *Journal of Fluid Mechanics*, Vol. 606, pp 369-397, (2008).

[4] A. K. Saha, G. Biswas, K. Muralidhar, Three-dimensional study of flow past a square cylinder at low Reynolds numbers, *International Journal of Heat and Fluid Flow*, Vol. 24, pp 54-66, (2003).

[5] Sohankar, C. Norberg, and L. Davidson, Simulation of three-dimensional flow around a square cylinder at moderate Reynolds numbers, *Physics of Fluids*, Vol. 11, pp 288-306, (1999).

[6] Sharma and V. Eswaran, Heat and fluid flow across a square cylinder in the two-dimensional laminar flow regime, *Numerical Heat Transfer, Part A: Applications*, Vol. 45, pp 247-269, (2004).